# Importance of radiative pumping for the excitation of the H2O submillimeter lines in galaxies

N.B. When citing this work, cite the original published paper.

(article starts on next page)

**Astronomy**
**&**
**Astrophysics**

LETTER TO THE EDITOR

# Importance of radiative pumping for the excitation of the H₂O submillimeter lines in galaxies

Eduardo González-Alfonso[1], Jacqueline Fischer[2], Javier R. Goicoechea[3], Chentao Yang[4],
Miguel Pereira-Santaella[5], and Kenneth P. Stewart[2]

[1] Universidad de Alcalá, Departamento de Física y Matemáticas, Campus Universitario, 28871 Alcalá de Henares, Madrid, Spain
   e-mail: eduardo.gonzalez@uah.es
[2] George Mason University, Department of Physics & Astronomy, MS 3F3, 4400 University Drive, Fairfax, VA 22030, USA
[3] Instituto de Física Fundamental (IFF), CSIC. Calle Serrano 121-123, 28006 Madrid, Spain
[4] Department of Earth and Space Sciences, Chalmers University of Technology, Onsala Observatory, 439 94 Onsala, Sweden
[5] Centro de Astrobiología (CSIC-INTA), Ctra. de Ajalvir, km. 4, 28850 Torrejón de Ardoz, Madrid, Spain

## ABSTRACT

H₂O submillimeter emission is a powerful diagnostic of the molecular interstellar medium in a variety of sources, including low- and high-mass star-forming regions of the Milky Way, and from local to high-redshift galaxies. However, the excitation mechanism of these lines in galaxies has been debated, preventing a basic consensus on the physical information that H₂O provides. Radiative pumping due to H₂O absorption of far-infrared photons emitted by dust and collisional excitation in dense shocked gas have both been proposed to explain the H₂O emission. Here we propose two basic diagnostics to distinguish between the two mechanisms: First, the ortho-H₂O $3_{21} - 2_{12}$ 75 μm and the para-H₂O $2_{20} - 1_{11}$ 101 μm rotational lines in shock-excited regions are expected to be in emission, while when radiative pumping dominates, the two far-infrared lines are expected to be in absorption. Second, the radiative pumping scenario predicts, based on the statistical equilibrium of H₂O level populations, that the apparent isotropic net rate of far-infrared absorption in the $3_{21} \leftarrow 2_{12}$ (75 μm) and $2_{20} \leftarrow 1_{11}$ (101 μm) lines should be higher than or equal to the apparent isotropic net rate of submillimeter emission in the $3_{21} \rightarrow 3_{12}$ (1163 GHz) and $2_{20} \rightarrow 2_{11}$ (1229 GHz) lines, respectively. Applying both criteria to all 16 galaxies and several Galactic high-mass star-forming regions in which the H₂O 75 μm and submillimeter lines have been observed with *Herschel*/PACS and SPIRE, we show that in most (extra)galactic sources, the H₂O submillimeter line excitation is dominated by far-infrared pumping, combined in some cases with collisional excitation of the lowest energy levels. Based on this finding, we revisit the interpretation of the correlation between the luminosity of the H₂O 988 GHz line and the source luminosity in the combined Galactic and extragalactic sample.

**Key words.** radiative transfer – line: formation – ISM: molecules – galaxies: ISM – infrared: galaxies – submillimeter: galaxies

## 1. Introduction

Soon after the launch of the *Herschel* Space Observatory (Pilbratt et al. 2010), spectroscopic observations with the SPIRE instrument (Griffin et al. 2010) revealed strong H₂O submillimeter (hereafter submm) emission from the ultraluminous infrared galaxy (ULIRG) Mrk 231, with strengths comparable to the those of the CO lines (van der Werf et al. 2010). The H₂O submm lines were subsequently detected in a variety of local galaxies with SPIRE (see Yang et al. 2013; Lu et al. 2017, and references therein) and HIFI (Liu et al. 2017), as well as in high-redshift ULIRGs and hyper-LIRGs from ground-based facilities (e.g., Omont et al. 2011, 2013; van der Werf et al. 2011; Yang et al. 2016, 2019). Based on the H₂O line fluxes in galaxies at all redshifts, Omont et al. (2013) and Yang et al. (2013) found a strong correlation, $L_{\mathrm{H_2O-submm}} \propto L_{\mathrm{IR}}^{\alpha}$, between the H₂O line luminosities and the infrared (IR) luminosities of the galaxies, with an index $\alpha$ slightly higher than unity. The extragalactic H₂O submm emission has been modeled in terms of radiative pumping (González-Alfonso et al. 2010, 2014, 2021; Pereira-Santaella et al. 2017), and the $L_{\mathrm{H_2O-submm}} - L_{\mathrm{IR}}$

correlations appeared to support this view (Omont et al. 2013; Yang et al. 2013; Lu et al. 2017).

In parallel, several H₂O submm lines have been observed in a large number of both low-mass and high-mass star-forming regions (LMSFR and HMSFRs) in our Galaxy (e.g., van Dishoeck et al. 2021, and references therein) with the HIFI instrument (de Graauw et al. 2010). The lines were resolved with the high spectral resolution provided by HIFI, showing broad profiles characteristic of outflows and their associated dense shocked gas in which the H₂O submm emission is excited by collisions. The H₂O line profiles also often showed a narrower spike at central velocities, which contributes negligibly (often in absorption) to the integrated emission in LMSFRs (e.g., Kristensen et al. 2012), but accounts for ~40% on average in HMSFRs (San José-García et al. 2016) and is attributed to the warm, massive envelopes around the luminosity sources. Considering both Galactic and extragalactic sources, San José-García et al. (2016) found a strong $L_{\mathrm{H_2O-submm}} - L_{\mathrm{IR}}$ correlation with an index $\alpha$ that was higher (and closer to unity) than when only the Galactic sources were fitted.

Using Infrared Space Observatory (ISO, Kessler et al. 1996) data (with 80″ aperture) and radiative transfer models, Cernicharo et al. (2006) found that much of the $H_2O$ line excitation in the Orion KL outflow is driven by the dust continuum radiation. On the other hand, van Dishoeck et al. (2021) argued, based on the nearly linear ($\alpha = 0.95 \pm 0.02$) correlation they found between *Herschel* $H_2O$ $2_{02}-1_{11}$ 988 GHz line luminosities of both Galactic and extragalactic sources vs. source luminosity, that the $H_2O$ submm emission in galaxies may be a scaled-up version of Galactic sources, where the $L_{H_2O-submm}-L_{IR}$ correlation is set by $H_2O$ collisional excitation in dense shocks.

In this Letter we address this lack of consensus on the excitation mechanism of these lines in galaxies, and thus on the physical information that $H_2O$ provides on the sources from which the $H_2O$ emission lines arise. We propose both a qualitative and a quantitative diagnostic to distinguish between the two mechanisms, each involving the far-infrared (far-IR) $H_2O$ $3_{21} - 2_{12}$ 75 μm and $2_{20} - 1_{11}$ 101 μm lines, and apply them to all extragalactic sources and a sample of HMSFRs where the $H_2O$ 75 μm and 1163 GHz lines have been observed with *Herschel*/PACS (Poglitsch et al. 2010) and SPIRE, respectively. A flat $\Lambda$CDM cosmology with $H_0 = 70\,\mathrm{km\,s^{-1}\,Mpc^{-1}}$ and $\Omega_M = 0.27$ is adopted, but for some nearby galaxies preferred distances are used.

## 2. Diagnostics

The simplified energy level diagram of Fig. 1a illustrates the basic mechanism of radiative pumping: if a 75 μm photon emitted by dust pumps an ortho-$H_2O$ molecule from the $2_{12}$ level to the $3_{21}$ one, it can relax via cascade down along the $3_{21} \rightarrow 3_{12} \rightarrow 3_{03} \rightarrow 2_{12}$ ladder through emission in the corresponding 1163, 1097, and 1717 GHz lines. Likewise, a pumping event in the para-$H_2O$ $2_{20} \leftarrow 1_{11}$ 101 μm line followed by cascade down along the $2_{20} \rightarrow 2_{11} \rightarrow 2_{02} \rightarrow 1_{11}$ ladder generates $H_2O$ emission in the 1229, 752, and 988 GHz lines. These can be denoted as "radiative pumping cycles", and always involve the loss of a continuum photon in the 75 and 101 μm pumping lines. Assuming that the absorption is isotropic, the 75 and 101 μm pumping lines will be seen in absorption. On the other hand, if $H_2O$ is collisionally excited (e.g., in dense shocks), the $3_{21}$ and $2_{20}$ levels will be populated accordingly and subsequent spontaneous emission in the $3_{21} \rightarrow 2_{12}$ and $2_{20} \rightarrow 1_{11}$ transitions will generate emission, rather than absorption, in both the 75 and 101 μm lines. We can then establish the first qualitative criterion to distinguish between radiative pumping and collisional excitation of the $H_2O$ submm lines assuming isotropy: in the former case, the 75 and 101 μm lines are expected in absorption, while in the latter case they are expected in emission.

Caveats on the above diagnostic are related to geometry effects. Shock-excited gas could be in front of a strong continuum source that could ultimately generate line absorption at 75 and 101 μm in the direction of the observer. However, since $T_{gas}$ and $n_{H2}$, which determine the excitation in shocks, are fully decoupled from the properties of the continuum source behind (and specifically $T_{gas} > T_{dust}$), fine tuning of the shock model would be required to obtain the absorption/emission pattern. On the other hand, lack of absorption in the 75 and 101 μm lines does not fully preclude the radiative pumping mechanism because the far-IR field responsible for the excitation might be external and might not impinge on the $H_2O$ molecules from the far side (in the direction of the observer), and hence would not produce line absorption (Appendix A in González-Alfonso et al. 2014).

A quantitative criterion for radiative pumping arises from the statistical equilibrium of the $H_2O$ levels: Because the populations of the $3_{21}$ and $2_{20}$ levels remain constant in time, and when we assume that their populations are exclusively determined by the above pumping cycles, the net rate of absorption events in the $3_{21} \leftarrow 2_{12}$ 75 μm line (hereafter $R^{abs}_{75\,\mu m}$) must be equal to the net rate of emission events in the $3_{21} \rightarrow 3_{12}$ 1163 GHz line ($R^{ems}_{1163\,GHz}$). Likewise, this equality holds for the para-$H_2O$ pumping cycle, $R^{abs}_{101\,\mu m} = R^{ems}_{1229\,GHz}$. We calculated $R^{ems,abs}_{line}$ in the limit of optically thin continuum emission at 75(101) μm and isotropic line absorption and emission,

$$R^{ems,abs}_{line}(s^{-1}) = \pm \frac{L_{line}}{E_{line}} = \pm 10^{-18} \frac{4\pi D_L^2 \, F_{line}}{(1+z)\,h\,c}, \tag{1}$$

where $E_{line} = h\nu_0$ is the energy of the line photons, $D_L$ is the luminosity distance, $z$ is the redshift, $h$ is the Planck constant, $c$ is the speed of light, and $L_{line}$ and $F_{line}$ are the line luminosity in erg s$^{-1}$ and line flux in Jy km s$^{-1}$ above (emission, + sign) or below (absorption, − sign) the continuum ($D_L$, $h$, and $c$ are in cgs units).

Equation (1) holds if the $H_2O$ 75(101) μm line is optically thick if it remains effectively optically thin such that repeated absorption and re-emission events in the line end with the photon either escaping from the source (without a contribution to $R^{ems,abs}_{line}$) or generating a submm cascade (contributing to both $R^{ems}_{line}$ and $R^{abs}_{line}$). However, if the far-IR continuum optical depth becomes significant, thermal continuum photons emitted at 75(101) μm will have a higher chance, after multiple line absorption and re-emission events, of being absorbed by dust grains before escaping from the source, generating absorption in the far-IR line without a submm line counterpart. In very optically thick regions (with continuum optical depths at 100 μm $\tau_{100} \gg 1$, as were found in a number of (U)LIRGs), the emission in the submm lines will be partially extincted and might even be observed in absorption. As $\tau_{100}$ increases, additional radiative paths (de)populating the $3_{21}$ and $2_{20}$ levels begin to play a role, but the overall general result is that the absorption fluxes of the 75 and 101 μm surface tracers are increased relative to the emission fluxes of the 1163 and 1229 GHz volume tracers. Therefore, in case of significant far-IR continuum optical depth effects, the $R^{ems,abs}_{line}$ rates calculated in Eq. (1) are only apparent, and we can more generally state that

$$R^{abs}_{75\,\mu m} \geq R^{ems}_{1163\,GHz} \tag{2}$$
$$R^{abs}_{101\,\mu m} \geq R^{ems}_{1229\,GHz}$$

are criteria for the radiative pumping mechanism in isotropic conditions. Anisotropy effects of the exciting radiation field could favor either $R^{abs}_{75\,101\,\mu m}$ or $R^{ems}_{1163,1229\,GHz}$, and would spread their relative values for randomly oriented sources.

The base levels from which the radiative pumping cycles operate, $2_{12}$ and $1_{11}$, must still be populated in some way. They could be populated via absorption of dust-emitted photons in the $2_{12} \leftarrow 1_{01}$ 179 μm and $1_{11} \leftarrow 0_{00}$ 269 μm ground-state lines, but this mechanism may be inefficient in optically thin $\tau_{100} < 1$ sources where the dust emission at these wavelengths is weak. At very high redshift, $H_2O$ excitation from the ground-state can also be produced by the cosmic microwave background (Riechers et al. 2022). Alternatively, the base levels could be excited through collisions in warm and dense regions, so that collisional excitation of the low-excitation lines combined with the radiative pumping mechanism would be required to account for the submm emission (González-Alfonso et al. 2014).
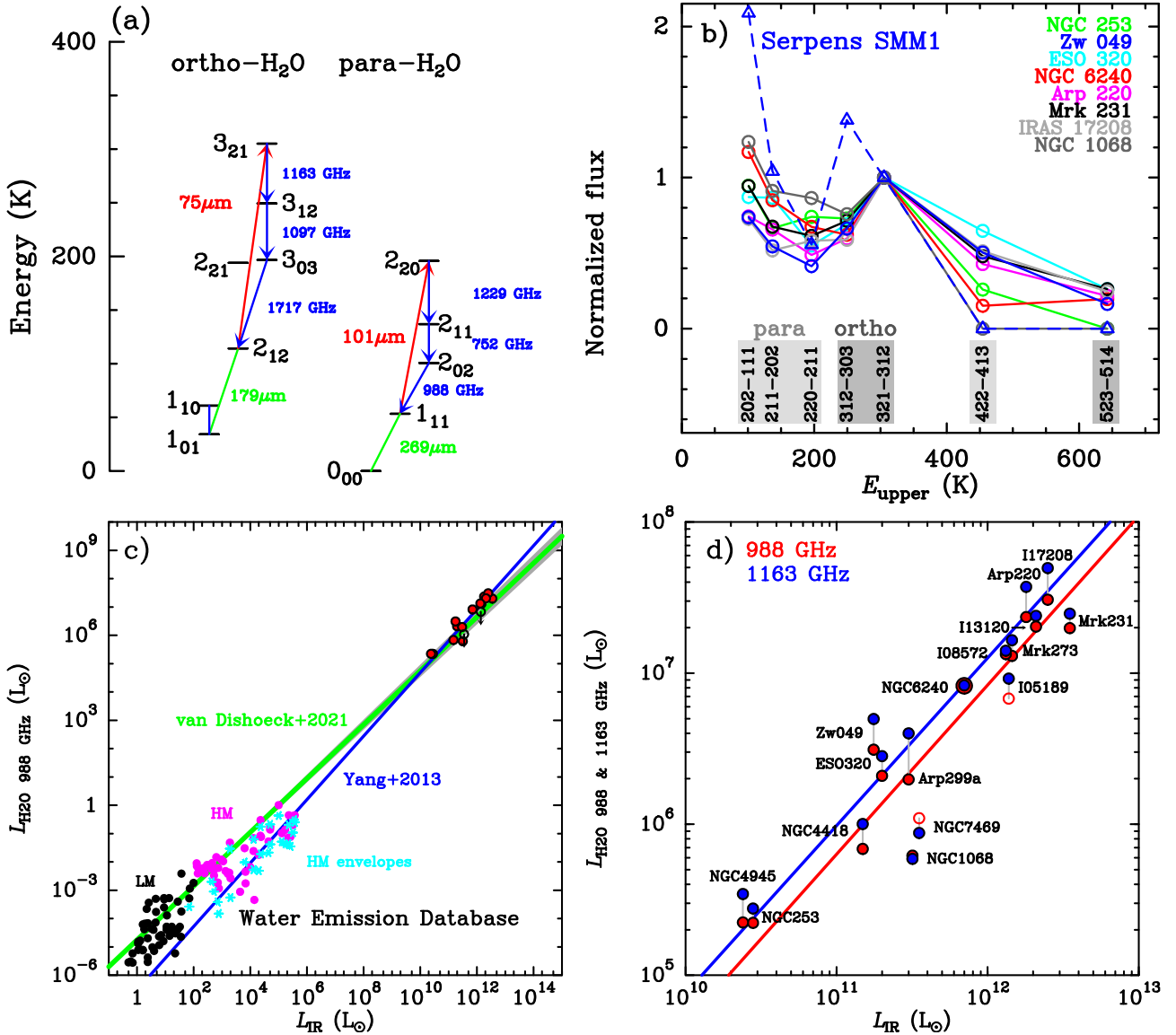
**Fig. 1.** H$_2$O submillimeter emission line relationships. *(a)* Simplified energy level diagram of ortho- and para-H$_2$O, illustrating the radiative pumping mechanism of H$_2$O submillimeter emission (Sect. 2). *(b)* Spectral line energy distribution of the H$_2$O submillimeter lines, normalized to the flux of the $3_{21} \rightarrow 3_{12}$ line, in eight extragalactic sources in which the pumping ortho-H$_2$O $3_{21} \leftarrow 2_{12}$ line at 75 μm has been observed, compared with the SLED in the LMSFR Serpens SMM1 (Goicoechea et al. 2012). The flux of undetected lines is set to 0. *(c)* Luminosity of the H$_2$O $2_{02} \rightarrow 1_{11}$ 988 GHz line as a function of the source IR luminosity for the extragalactic sources considered in this paper (red circles; open circles indicate 3σ upper limits) and the Galactic low-mass and high-mass star-forming regions (black and magenta circles, respectively, taken from the Water Emission Database; Dutkowska & Kristensen 2022; https://katarzynadutkowska.github.io/WED/). The light blue symbols isolate the contribution to $L_{\mathrm{H_2O\,988\,GHz}}$ by the envelopes of HMSFRs. The green line shows the best-fit power-law function to all Galactic and extragalactic sources found by van Dishoeck et al. (2021), with an index of 0.95 ± 0.02, and the blue line shows the fit found by Yang et al. (2013) to the extragalactic sources alone, with an index of 1.12. *(d)* Same as *(c)*, but zoomed-in on the extragalactic sources. The luminosity of the H$_2$O $3_{21} \rightarrow 3_{12}$ 1163 GHz line is added in blue. The red and blue lines show the fits by Yang et al. (2013).

## 3. Results

### 3.1. Extragalactic and Galactic samples

The crucial diagnostics for distinguishing between radiatively and collisionally excited H$_2$O submm emission rely on sensitive observations at 75 and 101 μm. We have applied them to all galaxies that have PACS observations covering the 75 μm line. This yielded a sample of 16 sources[1]. Line fluxes and details of the flux derivations will be presented in a forthcoming

paper (Fischer et al., in prep.). Unfortunately, the PACS gap at ~100 μm precluded observations covering the 101 μm line with *Herschel* in all galaxies but Mrk 231 (due to its redshift). This line, however, was detected with ISO in Arp 220 (Fischer et al. 2014).

The Galactic sample includes six well-known HMSFRs for which *Herschel*/PACS and SPIRE observations of the H$_2$O 75 μm and 1163 GHz lines are available: W31C and W49N (Gerin et al. 2015), W51 (Karska et al. 2014a), Sgr B2(M) and (N) (Etxaluze et al. 2013), and the Orion KL outflows (Goicoechea et al. 2015). In addition, the circumnuclear disk (CND) around Sgr A* (Goicoechea et al. 2013) was added. The

---

[1] With the exception of M 82, which is not detected in the 75 μm or in the 1163 GHz line and was therefore excluded from the sample.

flux of the $H_2O$ 75 μm line in this sample was extracted from the central $3 \times 3$ spaxels of PACS ($\approx 30'' \times 30''$). In Orion KL, we also measured the line flux in the direction of the hot core (hereafter HC; a very bright far-IR continuum source with a size of $\sim 10''$) within the central spaxel ($\approx 10'' \times 10''$), of the $H_2$ Peak 1 shocked-gas position ($\approx 30'' \times 30''$), and of Orion KL within a larger field of view (FoV of $\approx 120'' \times 120''$). The flux of the 1163 GHz line was extracted from similar apertures. The line profiles are displayed in Appendix A.

Our extragalactic sample includes a variety of well-known local (U)LIRGs: a quasi-stellar object (Mrk 231), active galactic nuclei (AGNs) such as IRAS 05189−2524, NGC 1068, NGC 7469, NGC 4945, IRAS 08572+3915, and NGC 6240 (the latter with strong CO emission associated with shocks; see Meijerink et al. 2013), (U)LIRGs with a compact obscured nucleus (NGC 4418, Arp 299a, Zw 049.057, ESO 320−G030, Mrk 273, Arp 220, and IRAS 17208−0014), and starburst galaxies (NGC 253 and IRAS 13120−5453). As delineated by the equivalent width of the OH 65 μm doublet (Fischer et al. 2014; González-Alfonso et al. 2015), the far-IR molecular absorption features are generally weak (EQW(OH 65 μm) < 20 km s$^{-1}$) while the emission in the atomic and ionic fine-structure lines is usually strong in six galaxies (NGC 1068, NGC 7469, NGC 253, NGC 6240, IRAS 13120−5453, and NGC 4945). They are referred to as emission-dominated galaxies (EDGs). The remaining galaxies (with EQW(OH 65 μm) > 20 km s$^{-1}$) have stronger far-IR molecular absorption features and are referred to as absorption-dominated galaxies (ADGs).

The extragalactic $H_2O$ submm spectral line energy distributions (SLEDs), in which the line fluxes are normalized to that of the $3_{21} \rightarrow 3_{12}$ 1163 GHz line (Fig. 1b), show a rather common $U$-shaped pattern for the low-excitation ($E_{up} \lesssim 300$ K) lines: The 1163 GHz line is usually the strongest line, followed by the 988 GHz line, except in NGC 1068, NGC 6240, and probably NGC 7469, in which this order is reversed. This strongly suggests that there is a common dominant excitation mechanism in all sources, but with variations. By contrast, the submm SLED in the LMSFR Serpens SMM1 (a template of collisional excitation in dense shocked gas; e.g., Goicoechea et al. 2012) looks different: The fluxes of the para- and ortho- lines sharply decrease with increasing $E_{up}$.

Figure 1c shows that most of the targets lie close to the $L_{H_2O-988\,GHz}-L_{IR}$ correlations found by Yang et al. (2013; for extragalactic sources) and van Dishoeck et al. (2021; for Galactic and extragalactic sources), and can thus be considered a representative sample of (mostly) (U)LIRGs. A closer inspection (Fig. 1d) reveals that NGC 7469 and NGC 1068 have high deficits in the emission of the $H_2O$ 988 GHz ($2_{02} - 1_{11}$) and mostly the 1163 GHz ($3_{21} - 3_{12}$) lines relative to the best global $L_{H_2O}-L_{IR}$ fit by Yang et al. (2013), with departures of $\gtrsim 3$. Together with NGC 6240, these sources also have the lowest 1163 GHz/988 GHz flux ratio.

### 3.2. Qualitative criterion

Of the 16 galaxies, 14 (87%) show the $H_2O$ 75 μm far-IR line in absorption (and the 101 μm line in Mrk 231 and Arp 220). The other two sources, NGC 1068 and NGC 7469, are ambiguous because the 75 μm is not detected at the $3\sigma$ level. The 75 μm spectrum of NGC 1068 is displayed in Appendix C, showing indications of a P Cygni profile in which the blueshifted negative flux nearly cancels out the redshifted positive flux.

In Galactic HMSFRs, the $H_2O$ 75 μm line is observed in absorption in all sources except for Orion KL (Fig. A.1). In Orion KL, the nature of the line depends on the specific observed region and FoV: the 75 μm line is observed in absorption toward the HC within the central PACS spaxel, but shows a P Cygni profile or is observed in emission for larger FoVs and toward Peak 1 (Fig. A.1).

By contrast, observations of low-mass class 0 and I and intermediate-mass protostars in which $H_2O$ is collisionally excited in shocks show the $H_2O$ far-IR lines (including the 75 μm line when observed, and with the exception of the 179 μm line in some sources) in emission (Herczeg et al. 2012; Goicoechea et al. 2012; Karska et al. 2014b, 2018; Matuszak et al. 2015).

### 3.3. Quantitative criterion

Figure 2a shows $R_{1163\,GHz}^{ems}$ as a function of $R_{75\,μm}^{abs}$ for the two samples, and Fig. 2b zooms in on the extragalactic sources. We categorize the galaxies in this plane into three groups according to the $r \equiv R_{75\,μm}^{abs}/R_{1163\,GHz}^{ems}$ ratio (see also the upper insert of Fig. 2a): $G_1$: 9 galaxies show $r > 1.4$; $G_2$: 5 sources lie within the calibration uncertainties close to the $R_{75\,μm}^{abs} = R_{1163\,GHz}^{ems}$ line ($0.6 < r < 1.4$); and $G_3$: 2 galaxies, NGC 1068 and NGC 7469, have only upper limits in $R_{75\,μm}^{abs}$ and show much higher $R_{1163\,GHz}^{ems}$. With the exception of Zw 049.057, all ADGs belong to $G_1$, so that the plane of Fig. 2 can be used to distinguish between ADGs and EDGs from the observation of only two lines. On the other hand, most of the Galactic HMSFRs of our sample except for Orion KL lie close to the $R_{75\,μm}^{abs}/R_{1163\,GHz}^{ems} = 1$ line, with values ranging from 0.34 (W51) to 1.4 (SgrB2(M)), and can thus be classified as belonging to $G_2$. Orion HC shows an excess of $R_{75\,μm}^{abs}$ similar to $G_1$ sources, but when the FoV increases (KL $30'' \times 30''$ and $2' \times 2'$) or toward Peak 1, $R_{75\,μm}^{abs}$ becomes negative (i.e., it is observed in emission; see the lower insert in Fig 2a).

Overall, most of the (U)LIRGs and HMSFRs observed in the $H_2O$ 75 μm line (nearly) follow the prediction of Eq. (2) over nine orders of magnitude in $R_{1163\,GHz}^{ems}$, indicating that far-IR pumping is the essential ingredient for understanding the $H_2O$ submm emission, and specifically, it dominates the observed $H_2O$ $3_{21} - 3_{12}$ 1163 GHz emission (and thus also the $3_{12} - 3_{03}$ 1097 GHz emission) in the majority of sources. In some galaxies and HMSFRs, there is an excess of submm emission over far-IR absorption ($R_{75\,μm}^{abs}/R_{1163\,GHz}^{ems} = 0.34-1$), which might either reflect a contribution to the submm line flux by shock-excited $H_2O$ or specific geometrical effects.

Multicomponent model fits to the emission and absorption fluxes of the SPIRE and the PACS $H_2O$ lines, and including the far-IR spectral energy distribution (SED), have been performed for most galaxies of our sample following the approach described in González-Alfonso et al. (2021; they will be presented in a forthcoming paper). Classification of the best-fit model components of each galaxy as optically thin when the optical depth of the continuum at 100 μm is lower than 1 ($\tau_{100} < 1$) and as optically thick if $\tau_{100} \geq 1$ shows in Fig. 2b that the $\tau_{100} < 1$ components (in gray) lie close to the $R_{75\,μm}^{abs} = R_{1163\,GHz}^{ems}$ line, as expected, while the optically thick components (in blue) predict weak emission in the 1163 GHz line, and the line even appears in absorption in some extreme nuclei. The ADGs have $R_{75\,μm}^{abs} > R_{1163\,GHz}^{ems}$ because buried components generate strong absorption in the $H_2O$ 75 μm, but little emission in the submm lines due to high continuum brightness and extinction
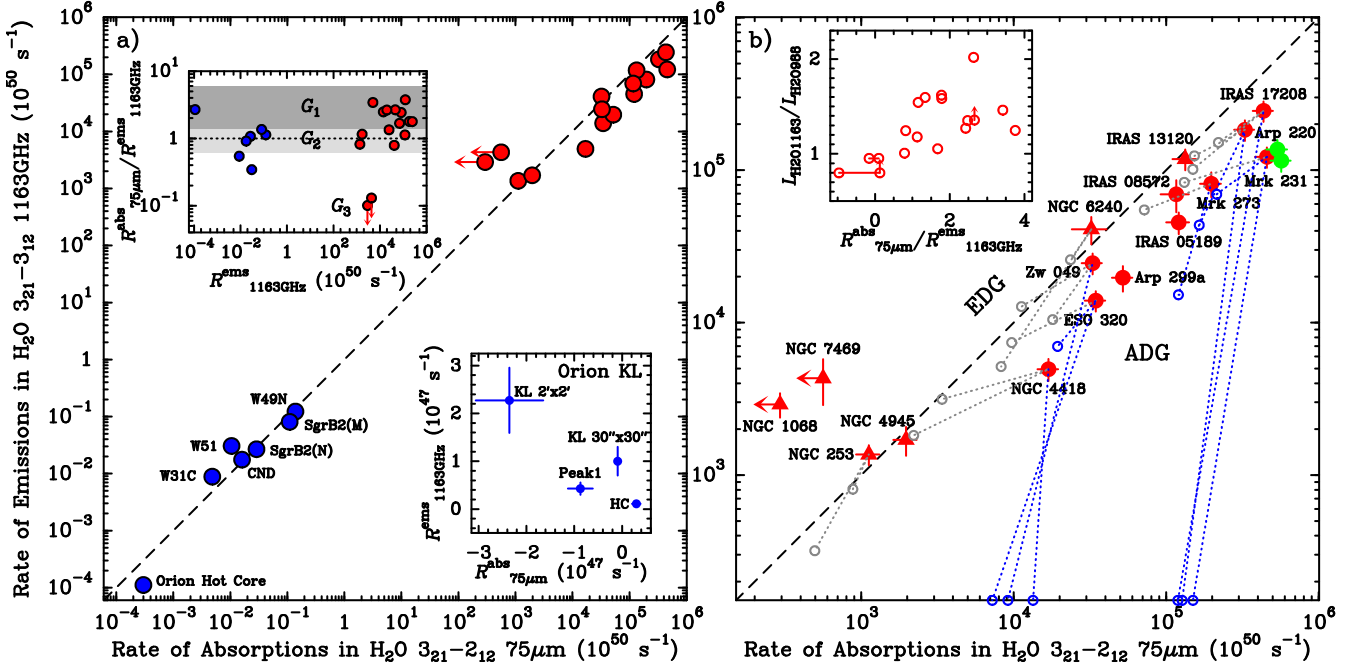
**Fig. 2.** Quantitative diagnostic of the radiative pumping mechanism. *(a)* Plot of $R_{1163\,\mathrm{GHz}}^{\mathrm{ems}}$ as a function of $R_{75\,\mu\mathrm{m}}^{\mathrm{abs}}$ for the Galactic and extragalactic samples. The dashed line indicates $R_{75\,\mu\mathrm{m}}^{\mathrm{abs}} = R_{1163\,\mathrm{GHz}}^{\mathrm{ems}}$. The lower insert shows these values in linear scale for Orion KL, with negative numbers of $R_{75\,\mu\mathrm{m}}^{\mathrm{abs}}$ indicating emission in the 75 μm line. The upper insert shows $r \equiv R_{75\,\mu\mathrm{m}}^{\mathrm{abs}}/R_{1163\,\mathrm{GHz}}^{\mathrm{ems}}$ vs. $R_{1163\,\mathrm{GHz}}^{\mathrm{ems}}$. Shading indicates the $G_1$, $G_2$, and $G_3$ groups defined according to the value of $r$ (Sect. 3.3). *(b)* Same as *(a)*, but zoomed-in on the extragalactic sources. Circles and triangles indicate ADGs and EDGs, respectively (Sect. 3.1). The green symbols show the same values, but for the $2_{02} \to 1_{11}$ (emission) vs. the $2_{20} \leftarrow 1_{11}$ (absorption) in the two sources (Mrk 231 and Arp 220) in which the 101 μm line has been observed. The open circles show the position in this plane of the optically thin ($\tau_{100} < 1$, in gray) and optically thick ($\tau_{100} > 1$, in blue) model components used to fit the H₂O emission and absorption (Appendix B). The insert shows the $3_{21} \to 3_{12}$-to-$2_{02} \to 1_{11}$ luminosity ratio vs. $R_{75\,\mu\mathrm{m}}^{\mathrm{abs}}/R_{1163\,\mathrm{GHz}}^{\mathrm{ems}}$, and horizontal segments indicate the most likely ranges for the two sources that are undetected in H₂O 75 μm.

in the submm. The submm lines, in contrast, are formed in optically thin (or moderately thick) and more extended regions, likely the 0.1−0.5 kpc circumnuclear disks of (U)LIRGs.

In Appendix B we compare the observed submm SLEDs of eight sample galaxies and the best-fit predictions by the multicomponent models, which generally agree well. We also show that in some EDGs (NGC 6240 and NGC 253), collisional excitation of the base levels is required to make the radiative pumping mechanism operational, and finally, we discuss in Appendix C whether the cases of NGC 7469 and NGC 1068 represent sources in which H₂O is excited by collisions in shocks or if geometrical effects can account for the lack of H₂O 75 μm absorption.

## 4. Discussion and conclusions

The preponderance of H₂O 75 μm absorption is difficult to reconcile with collisional excitation in shock cavities that are devoid of a significant amount of warm dust. An alternative is to assume that the H₂O 1163 GHz line is generated in an ensemble of shock cavities, in which the H₂O 75 μm line is also generated in emission, while a spatially separated and unrelated $\tau_{100} \gg 1$ component produces the 75 μm absorption (almost always stronger than the emission, which is required to generate net absorption in the line). However, this scenario does not explain the correlation between $R_{75\,\mu\mathrm{m}}^{\mathrm{abs}}$ and $R_{1163\,\mathrm{GHz}}^{\mathrm{ems}}$ as the two lines are generated in different regions and by different mechanisms. Even if $\dot{E}$ (mechanical) and $L_{\mathrm{IR}}$ are related, the specific lines respond in different ways to the far-IR and mechanical feedback. The case

of Orion KL illustrates this point: Large FoVs show emission in the 75 μm line far above the absorption toward the HC (lower insert in Fig. 2a).

The following interpretation of the $L_{\mathrm{H2O\,988\,GHz}} - L_{\mathrm{IR}}$ correlation stems from the present analysis. In Fig. 1c we have increased the dynamic range of the correlation found by Yang et al. (2013) for extragalactic sources to the luminosities characteristic of Galactic sources, assuming that the radiative pumping slope of 1.12 holds. Then, a number of HMSFRs and basically all LMSFRs, in which H₂O is excited by shocks, lie well above this line. Using the spectral decomposition of the H₂O 988 GHz spectra in HMSFRs carried out by van der Tak et al. (2013) and San José-García et al. (2016), we plotted in Fig. 1c the H₂O 988 GHz luminosities due to the massive envelopes of HMSFRs (light blue symbols) alone. The match with the extended extragalactic correlation was good. We thus propose that these Galactic massive envelopes (including the CND of the Milky Way) play a role similar to the circumnuclear disks in galaxies, where the H₂O submm emission is radiatively pumped[2]. This is combined at least in some cases with collisional excitation of the low-energy levels. Dominance of H₂O line excitation by collisions in dense shocks is proposed in Galactic sources located significantly above the blue line in Fig. 1c. The location of the Galactic HMSFRs in Fig. 2a resemble the starburst galaxies NGC 253 and IRAS 13120-5453,

---

[2] In this framework, the slope of 1.1 could be due to the increasing linewidth $\Delta v$ with $L_{\mathrm{IR}}$, as for the optically thick 75 and 101 μm lines $R_{75-101\,\mu\mathrm{m}}^{\mathrm{abs}} \propto \Delta v$. If $\Delta v$ increases by a factor $\sim 5$ as $L_{\mathrm{IR}}$ increases by 7 dex, the index of the correlation is $\sim 1 + (\log_{10} 5)/7 = 1.1$.

lacking an obscured nucleus that in its prominent form is a unique feature of extragalactic sources.

While we expect that the para-$H_2O$ 101 μm pumping cycle is as important as the ortho-$H_2O$ 75 μm cycle, the low-excitation $1_{11}$ and $2_{02}$ levels will be more affected by collisions in warm and dense regions than the $3_{21}$ level. The 988 GHz line is therefore less suitable than the 1163 GHz line for distinguishing between the two mechanisms.

# References

Cernicharo, J., Goicoechea, J. R., Daniel, F., et al. 2006, ApJ, 649, L33
de Graauw, T., Helmich, F. P., Phillips, T. G., et al. 2010, A&A, 518, L6
Dutkowska, K. M., & Kristensen, L. E. 2022, A&A, in press, https://doi.org/10.1051/0004-6361/202243235
Etxaluze, M., Goicoechea, J. R., Cernicharo, J., et al. 2013, A&A, 556, A137

Falstad, N., González-Alfonso, E., Aalto, S., et al. 2015, A&A, 580, A52
Falstad, N., González-Alfonso, E., Aalto, S., & Fischer, J. 2017, A&A, 597, A105
Fischer, J., Abel, N. P., González-Alfonso, E., et al. 2014, ApJ, 795, 117
Gerin, M., Ruaud, M., Goicoechea, J. R., et al. 2015, A&A, 573, A30
Goicoechea, J. R., Cernicharo, J., Karska, A., et al. 2012, A&A, 548, A77
Goicoechea, J. R., Etxaluze, M., Cernicharo, J., et al. 2013, ApJ, 769, L13
Goicoechea, J. R., Chavarría, L., Cernicharo, J., et al. 2015, ApJ, 799, 102
González-Alfonso, E., Fischer, J., Isaak, K., et al. 2010, A&A, 518, L43
González-Alfonso, E., Fischer, J., Aalto, S., & Falstad, N. 2014, A&A, 567, A91
González-Alfonso, E., Fischer, J., Sturm, E., et al. 2015, ApJ, 800, 69
González-Alfonso, E., Pereira-Santaella, M., Fischer, J., et al. 2021, A&A, 645, A49
Griffin, M. J., Abergel, A., Abreu, A., et al. 2010, A&A, 518, L3
Hailey-Dunsheath, S., Sturm, E., Fischer, J., et al. 2012, ApJ, 755, 57
Herczeg, G. J., Karska, A., Bruderer, S., et al. 2012, A&A, 540, A84
Karska, A., Herpin, F., Bruderer, S., et al. 2014a, A&A, 562, A45
Karska, A., Kaufman, M. J., Kristensen, L. E., et al. 2018, ApJS, 235, 30
Karska, A., Kristensen, L. E., van Dishoeck, E. F., et al. 2014b, A&A, 572, A9
Kessler, M. F., Steinz, J. A., Anderegg, M. E., et al. 1996, A&A, 315, L27
Kristensen, L. E., van Dishoeck, E. F., Bergin, E. A., et al. 2012, A&A, 542, A8
Liu, L., Weiß, A., Perez-Beaupuits, J. P., et al. 2017, ApJ, 846, 5
Lu, N., Zhao, Y., Diaz-Santos, T., et al. 2017, VizieR Online Data Catalog: J/ApJS/230/1
Matuszak, M., Karska, A., Kristensen, L. E., et al. 2015, A&A, 578, A20
Meijerink, R., Kristensen, L. E., Weiß, A., et al. 2013, ApJ, 762, L16
Omont, A., Neri, R., Cox, P., et al. 2011, A&A, 530, L3
Omont, A., Yang, C., Cox, P., et al. 2013, A&A, 551, A115
Pereira-Santaella, M., González-Alfonso, E., Usero, A., et al. 2017, A&A, 601, L3
Pilbratt, G. L., Riedinger, J. R., Passvogel, T., et al. 2010, A&A, 518, L1
Poglitsch, A., Waelkens, C., Geis, N., et al. 2010, A&A, 518, L2
Riechers, D. A., Weiss, A., Walter, F., et al. 2022, Nature, 602, 58
San José-García, I., Mottram, J. C., van Dishoeck, E. F., et al. 2016, A&A, 585, A103
Spinoglio, L., Pereira-Santaella, M., Busquet, G., et al. 2012, ApJ, 758, 108
van der Tak, F. F. S., Chavarría, L., Herpin, F., et al. 2013, A&A, 554, A83
van der Werf, P. P., Isaak, K. G., Meijerink, R., et al. 2010, A&A, 518, L42
van der Werf, P. P., Berciano Alba, A., Spaans, M., et al. 2011, ApJ, 741, L38
van Dishoeck, E. F., Kristensen, L. E., Mottram, J. C., et al. 2021, A&A, 648, A24
Yang, C., Gao, Y., Omont, A., et al. 2013, ApJ, 771, L24
Yang, C., Omont, A., Beelen, A., et al. 2016, A&A, 595, A80
Yang, C., Gavazzi, R., Beelen, A., et al. 2019, A&A, 624, A138

## Appendix A: $H_2O$ 75 μm profiles in Galactic high-mass star-forming regions
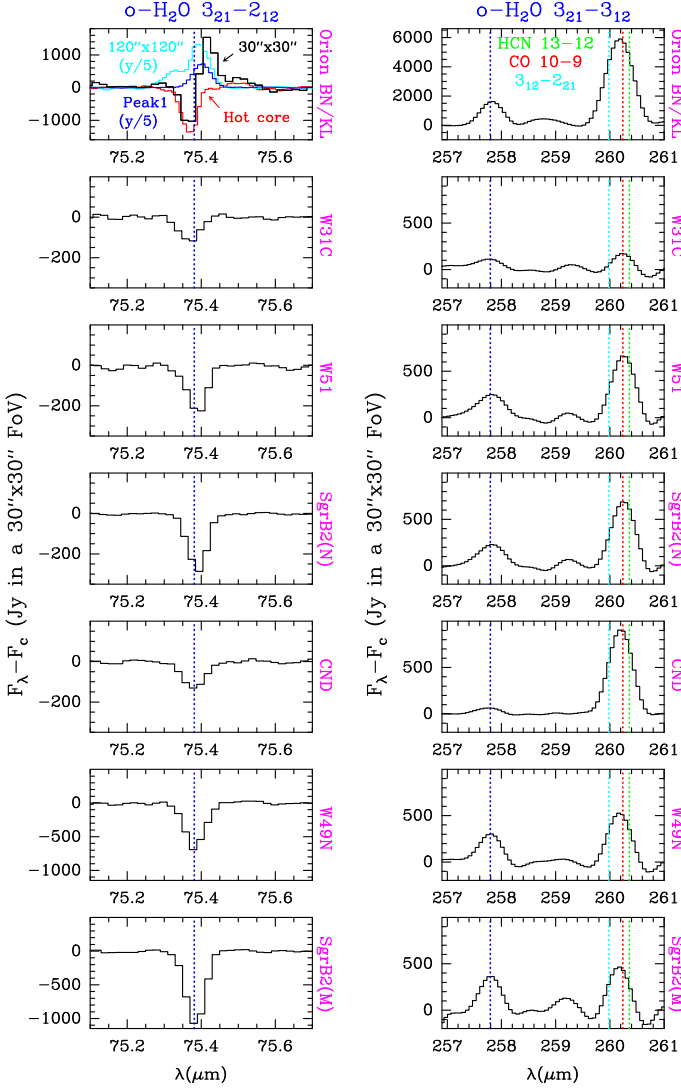


**Fig. A.1.** $H_2O\ 3_{21} - 2_{12}$ 75 μm (left) and $H_2O\ 3_{21} - 3_{12}$ 1163 GHz (right) profiles in seven Galactic high-mass star-forming regions, as observed with *Herschel*/PACS and SPIRE. The apodized SPIRE profiles also include the blend of CO 10-9 (which dominates the observed emission), $H_2O\ 3_{12} - 2_{21}$, and HCN 13-12. The PACS spectra correspond to the central $3 \times 3$ spaxels ($\approx 30'' \times 30''$). In Orion KL, the $H_2O$ 75 μm line is observed in absorption toward the HC, as seen within the central PACS spaxel ($\approx 10'' \times 10''$), but shows P Cygni and emission profiles for larger FoVs and toward Peak 1 (upper left panel; see also the insert in Fig. 2a).

Figure A.1 shows the $H_2O$ 75 μm and 1163 GHz profiles in our sample of Galactic high-mass star-forming regions.

## Appendix B: Submillimeter SLEDs

Figure B.1a compares the observed submm SLEDs with the best-fit predictions (in red) by the multicomponent models applied to eight sample galaxies, four (sub)LIRGs and four ULIRGs (see also Falstad et al. 2015, 2017, for similar models applied to Zw 049-057 and Arp 299a). In these models, collisional excitation was only roughly simulated with a single value of $T_{gas} = 150$ K and three values of the density ($n(H_2)$): $1.7 \times 10^4$,

$5 \times 10^4$, and $1.5 \times 10^5$ cm$^{-3}$ (González-Alfonso et al. 2021). Only in the case of NGC 6240 was the highest density favored for the component that dominates the $H_2O$ submm emission. The overall SLEDs are naturally reproduced with far-IR radiation fields that also account for the PACS lines and the SED, albeit with some discrepancies.

For the model components in Fig. B.1a, we used the same nomenclature (core, disk, and envelope) as in González-Alfonso et al. (2021). Schematically, the high-excitation absorption lines are formed in the far-IR photosphere of the optically thick and very warm cores; the medium-excitation absorption and emission lines have contributions from the disk components, and the envelopes dominate the $H_2O$ submm line emission and also generate some absorption in the low-excitation far-IR lines (such as the 75 μm line).

A general characteristic of the $H_2O$ submm SLEDs of galaxies is their $U-$shape, which is also shown in Fig. 1b. It is instructive to understand that according to our nonlocal models, the minimum emission line flux in most cases, which corresponds to the para-$H_2O\ 2_{20} - 2_{11}$ 1229 GHz line, is due to competing absorption of the continuum by the line in the optically thicker core and disk components, and not to an intrinsic weakness of the 1229 GHz line emission from the optically thin envelope. The absorption in the 1229 GHz line is strongest mainly because its $A_{ul}-$Einstein coefficient is 2.7× higher than that of the $2_{11} - 2_{02}$ 752 GHz line. Close to the source surface, this has the effect of reducing the excitation temperature ($T_{ex}$) of the 1229 GHz line, which will therefore be more prone to absorbing the brighter (because its frequency is also higher) continuum behind. The same effect does not occur with the ortho-$H_2O\ 3_{21} - 3_{12}$ 1163 GHz line because its $A_{ul}$ is only 1.2× higher than $A_{ul}(3_{12} - 3_{03}) + A_{ul}(3_{12} - 2_{21})$, and the 1163 GHz line therefore remains relatively excited (and even with suprathermal excitation in some models) close to the surface. The described absorption effect specific to the 1229 GHz line in ADGs is indeed clearly visible in our data: in Fig. 1b, Arp 220 (with a prominent core) shows one of the lowest (relative) 1229 GHz fluxes, while the EDGs NGC 1068 and NGC 253 do not show this dip. In summary, while the fluxes of the $H_2O$ submm lines are dominated by the envelopes, the cores and disks modulate the line ratios and generate the SLED $U-$shaped pattern.

In contrast with the nearly flat submm SLEDs for the envelopes predicted by the radiative pumping scenario (in absence of high collisional excitation of the low-excitation lines, see below), the SLED of Serpens SMM1[3] shows a strong decline in the fluxes of the para- and ortho-lines with increasing $E_{up}$ (Fig. 1b). Here, the dip in the para-$H_2O\ 2_{20} - 2_{11}$ 1229 GHz line has nothing to do with the absorption of any continuum, but with the difficulty of exciting the $2_{20}$ level without a continuum source emitting at 101 μm. A characteristic of $H_2O$ shock excitation in dense gas is that the ortho $3_{12} - 3_{03}$ 1097 GHz line is expected to be stronger than the $3_{21} - 3_{12}$ 1163 GHz line, as opposed to the situation when radiative pumping dominates.

For each of the eight sources, Fig. B.1b shows the predictions for the envelope component that dominates the $H_2O$ submm emission alone (gray symbols). To better understand the relative roles of collisional and radiative pumping, we generated exactly the same models, but quenched the collisional rates (in magenta).

---

[3] The Serpens SMM1 line fluxes were taken from Table A.1 of Goicoechea et al. (2012), with the exception of a few fluxes that appeared with typographical errors. The $H_2O\ 2_{20} - 2_{11}$ and $2_{21} - 1_{10}$ lines should have been listed as $1.46 \times 10^{-16}$ and $1.35 \times 10^{-15}$ W m$^{-2}$ instead of $2.92 \times 10^{-17}$ and $1.35 \times 10^{-16}$ W m$^{-2}$, respectively.
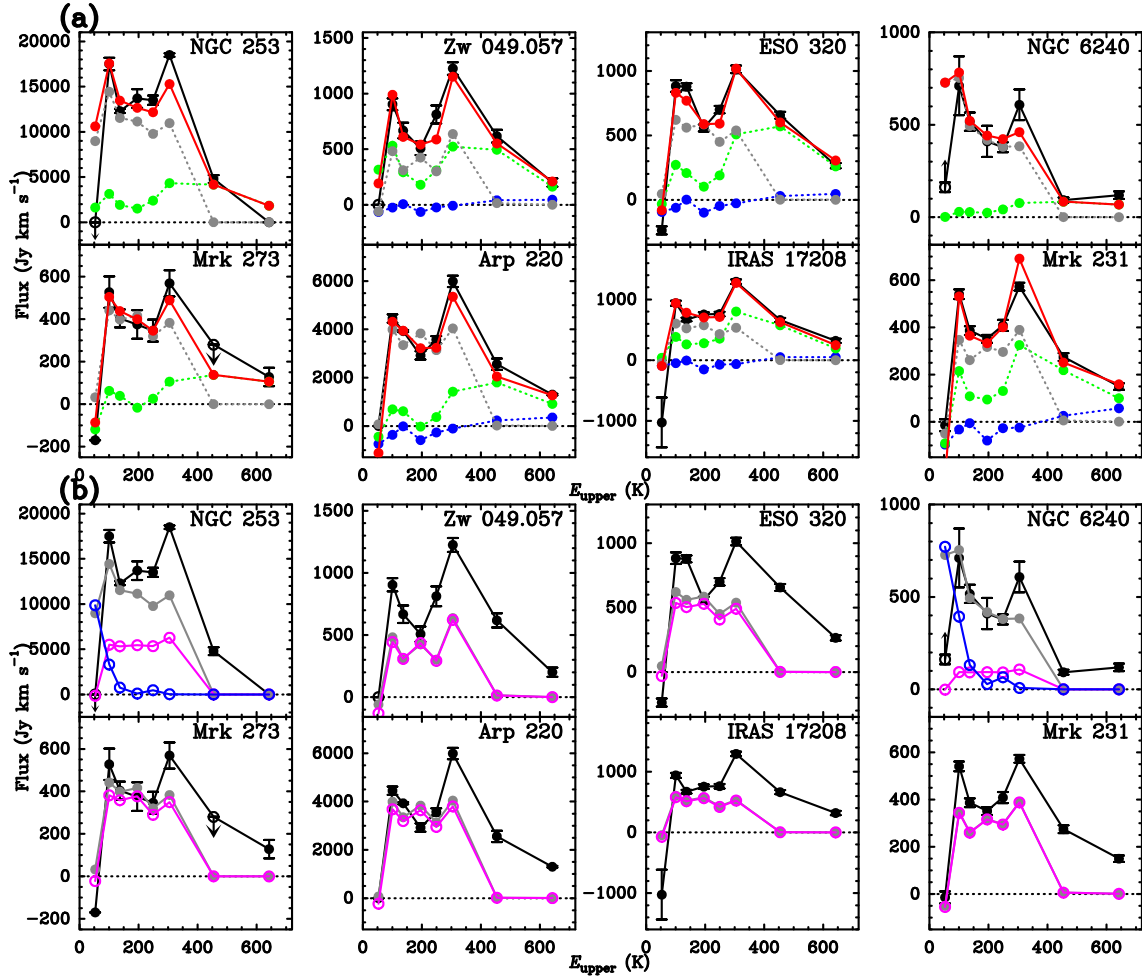
**Fig. B.1.** Model results for the $H_2O$ submm SLEDs. a) Fits to the $H_2O$ submm emission for eight local extragalactic sources analyzed in this paper, including all modeling components. Black circles with error bars show the observed fluxes. Blue, green, and gray circles indicate the contributions to the model fit by the core, disk, and envelope components, respectively, and red shows the total. b) Model component that dominates the emission of the $H_2O$ low-excitation submillimeter lines (the envelope component), shown with gray circles and lines. For comparison, magenta symbols and lines show the modeling results for these components that are obtained when the collisional excitation is quenched, and blue symbols (for NGC 253 and NGC 6240) indicate the results that are obtained when the far-IR pumping is quenched (but collisional excitation is included).

While the results in the four ULIRGs remain the same, meaning that collisional excitation has little effect on the $H_2O$ excitation, the quenching of collisions has a strong effect in some sub-ULIRGs, specifically, in NGC 253 and NGC 6240. In these EDGs, we also generated the same models, but quenched the pumping radiation field and kept the collisional excitation (in blue), with the result that the line fluxes dropped dramatically with the exception of the $1_{11} - 0_{00}$ and $2_{02} - 1_{11}$ lines. This indicates that collisional excitation is required to populate the base levels ($2_{12}$ and $1_{11}$) from which the pumping cycles operate (González-Alfonso et al. 2014). In these sources, the combination of collisional excitation of the base levels and radiative pumping from them generates the $H_2O$ submm emission. These results also suggest that in galaxies with the highest luminosities, collisional excitation of the base levels tends to be less important.

## Appendix C: Outliers (NGC 1068 and NGC 7469): Collisional excitation or geometrical effects?

NGC 1068 and NGC 7469 are ambiguous sources because the $H_2O$ 75 μm line is neither detected in absorption, as expected in the scenario of radiative pumping, nor in emission, as expected

in the case of shock excitation. As shown in Fig. 1d, both sources are underluminous in the $H_2O$ 1163 GHz and 988 GHz lines relative to $L_{IR}$, with a stronger deficit in the 1163 GHz line. These galaxies are thus not representative of the bulk of (U)LIRGs that are observed with SPIRE and were fit by Yang et al. (2013), but may well represent a population of low-luminosity AGNs ($\lesssim 10^{11} L_\odot$) with starburst rings, which are undersampled by *Herschel*/PACS and SPIRE.

The PACS continuum-subtracted spectrum around the $H_2O$ $3_{21} - 2_{12}$ 75 μm line in NGC 1068 is shown in Fig. C.1. The net flux of the line in NGC 1068 and NGC 7469 is below $3\sigma$ ($42 \pm 64$ and $73 \pm 30$ Jy km s$^{-1}$), but indications of a P Cygni profile are visible in the spectrum of NGC 1068, in which the absorption and emission features nearly cancel each other. P Cygni profiles with similar absorption and emission fluxes are characteristic of radiatively excited lines. We note that the redshifted emission component will also contribute to the 1163 GHz flux via radiative pumping without generating 75 μm absorption because the emitting gas is on the far side of the continuum source. This is one example of the anisotropy we discussed in Section 2. However, the measured flux in the 75 μm blueshifted absorption component falls too short to account for the observed strong submm emission in the 1163 GHz line.

Spinoglio et al. (2012) reported and analyzed the H$_2$O submm emission in NGC 1068, including the detected PACS lines (all in emission). The H$_2$O emission was found to be dominated by the CND around the AGN. Collisional excitation of H$_2$O is important in the CND, as indicated, for instance, by the relatively strong emission of the H$_2$O $1_{11} - 0_{00}$ 1113 GHz line and by the 1163-to-988 flux ratio, which is lower than 1 (Fig. 1b). However, the proposed LVG models that ignored radiative pumping yielded $T_{\rm gas} \sim 40$ K for the H$_2$O in the CND that did not match the conditions inferred from the CO lines ($T_{\rm gas} \sim 170 - 570$ K; Hailey-Dunsheath et al. 2012). An alternative model was then explored by González-Alfonso et al. (2014), which included the radiative pumping effect by the dust mixed with H$_2$O and also by an external far-IR radiation field that was anisotropic, that is, it did not impinge onto the clumps in the direction of the observer and thus did not produce absorption of the far-IR lines in the direction of the Earth. Conversely, the external field produced emission in the far-IR lines, which would almost cancel the absorption by the internal field in the case of the 75 μm line. A similar situation might be encountered in the Sy 1.2 galaxy NGC 7469.
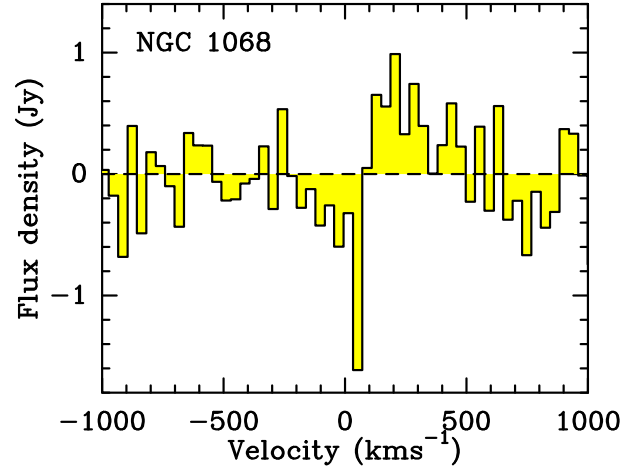


**Fig. C.1.** H$_2$O $3_{21} - 2_{12}$ 75 μm continuum-subtracted spectrum in NGC 1068.